

See discussions, stats, and author profiles for this publication at: <https://www.researchgate.net/publication/282551917>

# How Does Thermal Poling Produce Interstitial Molecular Oxygen in Silicate Glasses?

ARTICLE *in* THE JOURNAL OF PHYSICAL CHEMISTRY C · JULY 2015

Impact Factor: 4.77 · DOI: 10.1021/acs.jpcc.5b04513

---

READS

52

3 AUTHORS, INCLUDING:



Alexey Redkov

Saint Petersburg Academic University

11 PUBLICATIONS 9 CITATIONS

[SEE PROFILE](#)



Andrey Lipovskii

St. Petersburg State Polytechnical University

199 PUBLICATIONS 1,736 CITATIONS

[SEE PROFILE](#)

# How Does Thermal Poling Produce Interstitial Molecular Oxygen in Silicate Glasses?

Alexey V. Redkov,<sup>†,‡</sup> Vladimir G. Melehin,<sup>§</sup> and Andrey A. Lipovskii<sup>\*,†,||</sup>

<sup>†</sup>St. Petersburg Academic University RAS, Khlopina str., 8/3, Saint-Petersburg, 194021 Russia

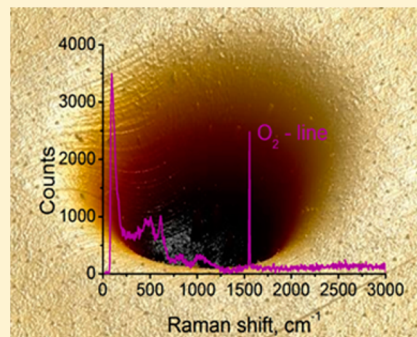
<sup>‡</sup>Institute of Problems of Mechanical Engineering, Bolshoy pr. V. O., 61, Saint-Petersburg, 199178 Russia

<sup>§</sup>A.F.Ioffe Physical-Technical Institute, Polytechnicheskaja 26, Saint-Petersburg, 194021 Russia

<sup>||</sup>Peter the Great St. Petersburg Polytechnic University, Polytechnicheskaja str., 29, Saint-Petersburg, 195251 Russia

## Supporting Information

**ABSTRACT:** Thermal poling of glasses induces structural and compositional modification and breaks central symmetry of these initially isotropic media. In spite of numerous experimental data accumulated, little is known about the processes occurring in soft glasses under this processing. We use micro-Raman technique to study the formation of interstitial molecular oxygen and structural modification of the subsurface layer of a soda-lime silicate glass in the course of thermal poling. The presence of O<sub>2</sub> is demonstrated in cation-depleted subanodic region of the glass, the thickness of which depends on the charge passed during the poling procedure and, in our experiments, reaches one micron. O<sub>2</sub> concentration in this layer is independent of the charge passed and is on the order of  $3 \times 10^{20} \text{ cm}^{-3}$  being maximal in anodic surface craters arising because of poling current nonuniformities. O<sub>2</sub> generation is accompanied by an increase in the concentration of three-membered Si—O rings in the modified region of the glass matrix. The ways of nonbridging oxygen recombination are discussed and proposed as the main mechanism of the interstitial O<sub>2</sub> formation.



## 1. INTRODUCTION

The procedure of the thermal polarization of a glass in a strong electric field introduced in the seventieth of the last century by Carlson<sup>1</sup> as “electrode polarization” nowadays is generally referred to as thermal poling. The essence of this procedure is applying of several hundred volts DC voltage to a glass plate placed between two conductors and heated up to a temperature sufficient to activate ionic conductivity. For conventional alkali silicate glasses, this temperature is about 200–300 °C, and it is noticeably less than the glass transition temperature, ~550 °C. Due to the electric field induced drift of positively charged alkali and alkaline earth ions (cations) from the subsurface glass region toward the bulk of the glass, a change in the composition and structure of the subanodic region of the glass occurs, and a layer of a negative space charge arises. A strong electric field in this layer results in breaking of central symmetry of the poled glass.<sup>2–4</sup> The changes in the composition and structure of the subanodic region of the glass under thermal poling<sup>5–7</sup> are accompanied by changes in the refractive index of this region,<sup>8,9</sup> formation of a relief on the surface of the glass near the edge of the anodic electrode or under the electrode if a profiled one is used,<sup>10–12</sup> and by a change in the rate of chemical etching relative to unpoled regions of the same glass.<sup>13</sup> A strong motivation of studies of glass poling was associated with the poling of silica optical fibers to provide their electrooptical sensitivity and optical nonlinearity.<sup>14,15</sup> To date, the use of glass

poling to manufacture optical waveguides<sup>16</sup> and diffraction gratings<sup>11,17</sup> has also been demonstrated.

Despite the large amount of accumulated data, physical processes occurring in the subanodic region of glasses under thermal poling are not completely understood yet. The registration of molecular oxygen in poled glasses was reported in several papers;<sup>12,18–20</sup> however, quantitative estimates of its concentration were not undertaken, and the mechanism of the interstitial O<sub>2</sub> formation is not clear yet. Initially, two main hypotheses explaining the appearance of O<sub>2</sub> in poled glasses were proposed. Both of them are based on the consideration of the process of charge transfer in the course of poling. In accordance with the first one (see ref 20 and references therein), the transfer of charge in the cation-depleted subanodic layer of a glass is provided by the drift of negatively charged oxygen ions toward the anode under a strong electric field. Reduction of these ions near the anodic electrode results in the formation of molecular oxygen. In accordance with the second hypothesis,<sup>21</sup> negative charge transfer in the cation-depleted layer is purely an electronic process, the electrons being generated in the discharge of negatively charged nonbridging oxygen atoms, while the oxygen atoms remain stationary and in some way recombine with O<sub>2</sub> formation.<sup>19</sup>

Received: May 11, 2015

Revised: July 6, 2015

The argument in favor of the oxygen ions drift<sup>20</sup> is anodic bonding phenomenon. The electronic charge transfer hypothesis can be supported by the detection of electrons contribution to glass conductivity in poling<sup>21</sup> and by the registration of molecular oxygen in a sufficiently thick,  $\sim 1 \mu\text{m}$ , subanodic layer of poled glasses,<sup>12,18,19</sup> not only in the close vicinity of the anodic electrode as supposed in ref 20. In the case of electron transport, the subanodic layer should be enriched with discharged nonbridging oxygen (NBO), while this enrichment is hardly possible if the transport of oxygen ions take place. If there are no complementary defects, like three-coordinated silicon, in the glass network, the high concentration of the discharged NBO makes possible the relaxation of the glass matrix, which is followed by the recombination of the NBO and interstitial molecular oxygen formation. It is worth noting that the interstitial oxygen can also appear in glasses after other types of modifications, like irradiation with high-energy electrons<sup>22</sup> or femtosecond laser pulses.<sup>23</sup>

This work is aimed at the study of the morphology of the anodic surface of thermally poled alkali silicate glasses, the characterization of compositional/structural changes in the poled glass depending on the charge passed in the poling, the evaluation of interstitial molecular oxygen concentration, and establishing of a possible mechanism of its formation. Experimental studies were performed using micro-Raman setup, optical microscopy, optical profilometry, and atomic force microscopy.

## 2. EXPERIMENTAL DETAILS

In the experiments, we used 1 mm thick soda-lime glass slides (Menzel microscope slides). This glass contains<sup>24</sup> 72.20% SiO<sub>2</sub>, 14.30% Na<sub>2</sub>O, 6.40% CaO, 4.30% MgO, 1.20% K<sub>2</sub>O, 1.20% Al<sub>2</sub>O<sub>3</sub>, 0.30% SO<sub>3</sub>, and 0.03% Fe<sub>2</sub>O<sub>3</sub>, in weight percent. Calculated atomic composition of this glass is presented in Table 1.

**Table 1. Atomic Composition of Menzel Microscope Slides**

element	concentration ( $10^{21} \text{ cm}^{-3}$ )
Si	17.95
O	43.55
Na	6.89
Ca	1.71
Mg	1.59
K	0.38
Al	0.35
S	0.6
Fe	0.006

Thermal poling of the slides was performed in the air at 250 °C and in applied voltage range of 100–2400 V. The list of studied samples and poling conditions that are maximal voltage and passed charge is shown in Table 2.

To avoid thermal breakdown, the voltage applied to the samples was increased in 50–100 V steps. For given voltage, we stopped the process and cooled the sample after the 10 times drop of poling current. The geometry of parallel-plate capacitor and polished n-silicon clamped electrodes of  $1 \times 1 \times 0.03 \text{ cm}^3$  in size were used because of high surface quality of industrial silicon wafers and good conductivity of the n-silicon plates. In principle, using other types of silicon should not influence the results of poling experiments. A good contact of the glass slide and the anodic electrode prevented interaction of the glass with

**Table 2. List of Prepared Samples and Poling Conditions**

sample no.	charge density (mC/cm <sup>2</sup> )	maximal voltage, V
3	59	600
5	128	1000
7	316	1540
8	364	1700
11	513	2000
12	670	2360

the atmosphere in the course of poling, and the anode was considered a blocking one.

In our experiments, passed charge density was calculated via integrating measured poling current versus time dependence divided by the electrode area. The glass surface morphology was studied using Zygo New View optical profilometer and Dimension 3100 (Veeco) atomic force microscope (AFM). For the excitation of Raman spectra, we used the wavelength of 532 nm. The spectrum was recorded using Witec Alpha 300R spectrometer equipped with a confocal microscope, which can construct three-dimensional Raman maps with a spatial resolution of  $\sim 1.5 \mu\text{m}$ . All Raman measurements were performed at room temperature.

## 3. RESULTS

**3.1. Surface Morphology.** As previous profilometric studies<sup>12</sup> of the anodic surface of poled glasses have shown, the surface under the electrode displaces relative to the surface of the unpoled regions of the glass because of the anodic electrode intrusion into the glass. This displacement increases with the charge passed through the sample in poling. It is important that the decrease of the glass volume corresponding to the measured intrusion exceeds one calculated within the frames of excluded volume model,<sup>25</sup> which accounts for the removal of alkali and alkali-earth atoms from the poled glass region. Therefore, it is suggested<sup>12</sup> that the additional contribution to the volume change is due to an increase in the polymerization of the glass under poling.

When the applied voltage exceeds 1000 V, the poling results in the appearance of multiple randomly placed craters about 5  $\mu\text{m}$  in size on the glass surface as shown in Figure 1a. This size allowed us using micro-Raman technique to study the craters. AFM measured profile of the surface in the region containing two craters is presented in Figure 1b, the depth of the craters for this sample being equal to  $\sim 350 \text{ nm}$ . 3D Image of one of the craters presented in Figure 1c evidences that its surface is smooth and the arisen nonuniformity of the surface is not a microcrack.

Apparently, the reason for the craters formation is an inhomogeneity of the poling current. Higher local current density provides a higher temperature and, respectively, a higher degree of polymerization of the matrix, which is followed by a more essential decrease in local glass volume that is the craters formation. Since the craters appear only at high voltage, above 1000 V, it can be assumed that the change in the current flow from uniform to inhomogeneous is not due to the quality of the contacts but because of the poling current instability arising at the high voltage applied.

**3.2. Raman Spectra.** The main attention in the study of Raman spectra of the subanodic glass region was paid to the thickness of the layer containing molecular oxygen and to the concentration of O<sub>2</sub>. Figure 2 shows measured outside and inside the craters spectra of the glass samples poled with

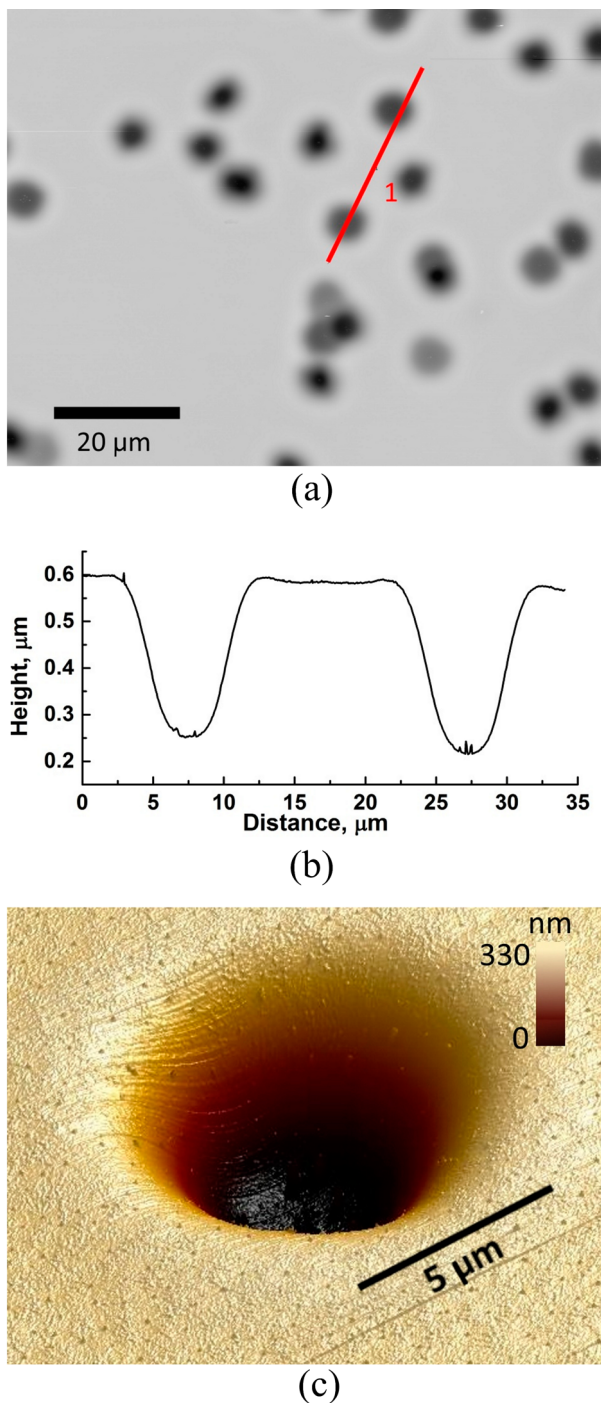


**Figure 1.** (a) Optical microscope image of a region containing multiple craters on the surface of sample no. 11, (b) AFM profile of the two craters along the line 1, and (c) 3D AFM image of a crater.

different charge density passed through. Each spectrum was recorded with focusing the microscope to the depth where the oxygen line intensity was maximal. For a comparison, the spectra of the original glass and fused silica are also shown.

The spectra of the samples contain three broad bands typical for silicate glasses:  $400\text{--}550\text{ cm}^{-1}$  (rocking mode of Si–O–Si bridges),  $700\text{--}850\text{ cm}^{-1}$  (bending mode of Si–O–Si bridges), and  $950\text{--}1250\text{ cm}^{-1}$  (asymmetric stretching vibrations of Si–O–Si bridges and Si–O nonbridging bonds in  $Q^n$  tetrahedral entities containing  $n$  bridging oxygen atoms per a silicon atom). The low-frequency Raman peak centered at  $\sim 150\text{ cm}^{-1}$ , the

amplitude of which grows with the transferred charge (e.g., Figure 2) is, for our opinion, because of Rayleigh scattering by nonuniformities in the poled region of the glass. These nonuniformities grow in poling and can be seen (e.g., in TEM images presented by An).<sup>6</sup> Being cut with the shutter positioned at  $\sim 100\text{ cm}^{-1}$ , the averaged remaining Rayleigh scattering spectrum looks like a peak.

In the initial glass, the most intense line in the band  $950\text{--}1250\text{ cm}^{-1}$  is the line at  $1100\text{ cm}^{-1}$  ( $Q^3$ ). In the spectra of the poled glasses, the line at  $605\text{ cm}^{-1}$  (D2, three membered rings) appears. The line at  $605\text{ cm}^{-1}$  is typical for silica glasses and associated with breathing mode of rings composed of three vertices-connected tetrahedrons.<sup>26</sup> The narrow line at  $1550\text{ cm}^{-1}$  in the spectra of the poled glasses corresponds to molecular oxygen.<sup>27,28</sup> Besides, this line was also observed after  $\beta$ -irradiation of glasses.<sup>29</sup> It should be noted that the line at  $495\text{ cm}^{-1}$ , which corresponds to D1 (four membered rings), was not observed in the spectra of the poled glasses. As it is seen in Figure 2, the most notable changes in the spectra are in the intensity of the glass matrix band at  $1100\text{ cm}^{-1}$  and the lines at  $605\text{ cm}^{-1}$  (D2) and  $1550\text{ cm}^{-1}$  ( $O_2$ ).

The intensity of the line at  $1100\text{ cm}^{-1}$  decreases with the increase in passed charge density while the D2 line and molecular oxygen line intensities increase. When the charge density exceeds  $300\text{ mC/cm}^2$ , the intensity of the molecular oxygen line becomes comparable with the most intensive band of the glass matrix at  $400\text{--}550\text{ cm}^{-1}$ . This was never previously observed. The ratio of the intensities of the D2 band and the matrix band at  $400\text{--}550\text{ cm}^{-1}$  also increases with the charge passed, indicating glass matrix densification. Note that 1 h annealing of the poled glass samples in air at  $400\text{ }^\circ\text{C}$  results in the disappearance of the  $O_2$  line from the spectra, that is molecular oxygen leaves the matrix.

The differences of the spectra measured in a flat region and in a crater are illustrated with Figure 3. Figure 3a presents the optical image of the surface with a few craters (sample no. 8), and Figure 3b and 3c show the maps of the intensity of the oxygen line at  $1550\text{ cm}^{-1}$  and the matrix band at  $1100\text{ cm}^{-1}$  in the selected area, respectively. As it is seen in Figure 3, the intensity of  $O_2$  line at the locations of craters is higher than outside of them, while the behavior of the matrix band is opposite. This decrease in the intensity of the matrix band at  $1100\text{ cm}^{-1}$  in the crater is due to a decrease in the polarizability of bonds in Si-tetrahedron within the sodium depleted region under the crater.

Figure 4 shows the dependence of the ratio  $i$  of the oxygen line intensity to the intensity of the matrix band at  $700\text{--}850\text{ cm}^{-1}$  in the spectra shown in Figure 2 versus the magnitude of the charge density passed through the samples in our experiments. This correlates with the transferred charge dependence of the spatial relief height formed in thermal poling,<sup>12</sup> and one can suppose similar nonlinear character of the dependence. This is because the confocal parameter of the focused beam in micro-Raman measurements sufficiently exceeds the thickness of the layer containing molecular oxygen, which is less than one micron. For using these data to evaluate  $O_2$  concentration, it is necessary, first, to make the calibration using an etalon, similar in composition and structure to the  $O_2$  enriched poled layer (to

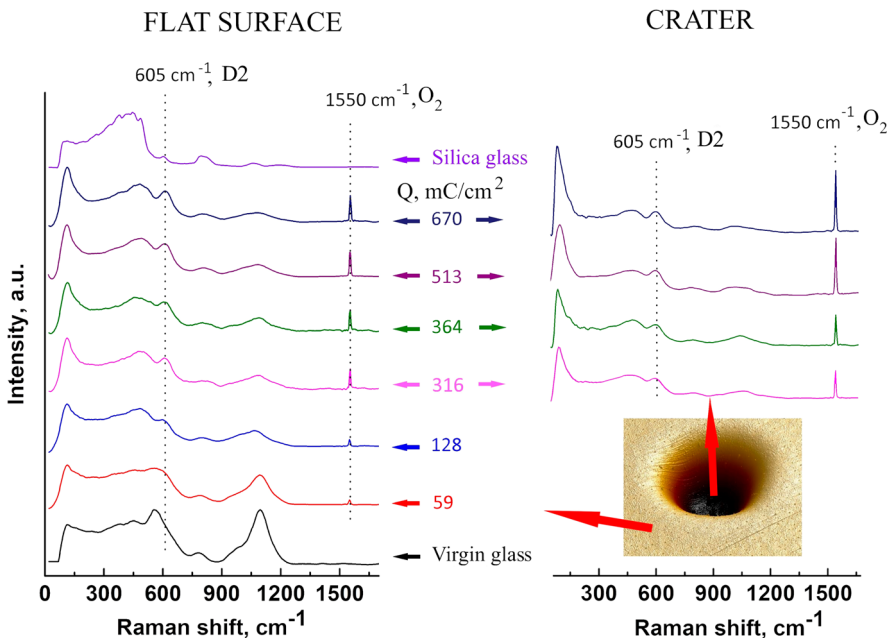


**Figure 2.** Raman spectra of poled samples differing in the density of passed charge corresponding to the flat surface and a crater. The spectra of virgin soda-lime glass and silica glass are presented for comparison.

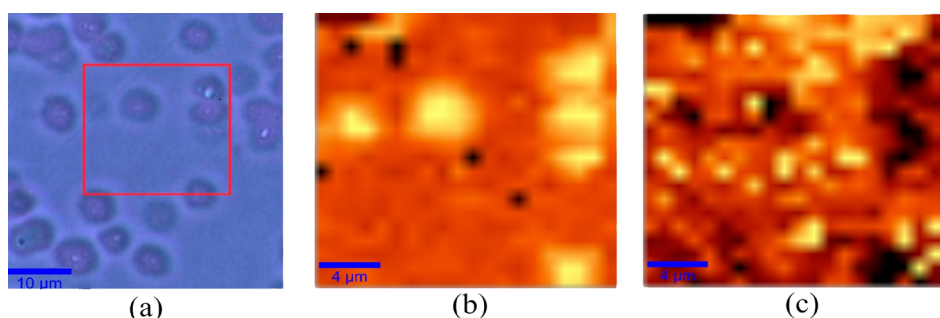


**Figure 3.** (a) Optical microscope image of a region of sample no. 8 and Raman maps of the marked area: (b) molecular oxygen line at  $1550\text{ cm}^{-1}$  and (c) glass matrix line at  $1100\text{ cm}^{-1}$ .

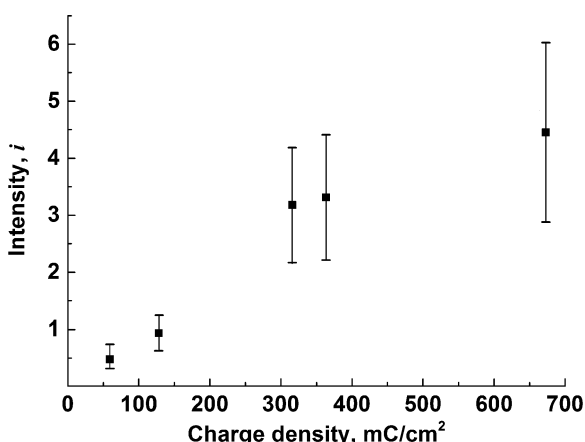


**Figure 4.** Ratio of the intensity  $i$  of the oxygen line at  $1550\text{ cm}^{-1}$  to the intensity of the glass matrix line at  $700\text{--}850\text{ cm}^{-1}$  vs the density of the passed charge.

consider the “crystal” field acting on the molecule of oxygen in the matrix as the same) with a known  $\text{O}_2$  concentration, and, second, to measure the thickness of this layer. For the calibration, we used evaluated content of the interstitial  $\text{O}_2$  in

Suprasil W1.<sup>30</sup> In accordance with ref 30, the ratio  $i$  for the Suprasil,  $i_{\text{Suprasil}} \approx 0.02$  at the concentration of  $\text{O}_2 n_0 \approx (8 \pm 3.5) \times 10^{17}\text{ cm}^{-3}$ . To determine the thickness of  $\text{O}_2$ -enriched layer, we performed chemical etching of the sample nos. 8 and 12, which demonstrated the highest intensity of the  $\text{O}_2$  line. The depth of the etching was measured using the profilometer. Raman spectra of sample no. 8 measured at several etching depths are presented in Figure 5. After each etching step, the microscope was focused to the maximal intensity of the  $\text{O}_2$  line.

As can be seen from Figure 5, the intensity of the lines corresponding to three-membered rings and  $\text{O}_2$  decrease with the thickness of the removed layer while the intensity of the matrix line at  $1100\text{ cm}^{-1}$  increases. When the thickness of the removed layer is  $\sim 650\text{ nm}$ , the Raman spectrum is close to one of the virgin glass. The ratio  $i$  versus the thickness of the removed layer is presented in Figure 6 for the sample nos. 8 and 12. As can be seen from that figure, these dependences are close to linear, that is the distribution of molecular oxygen in the subanodic glass layer is almost uniform. Thus, the increase in the relative intensity of  $\text{O}_2$  line in the spectra presented in Figure 2 is because of increasing thickness of the  $\text{O}_2$ -containing layer.

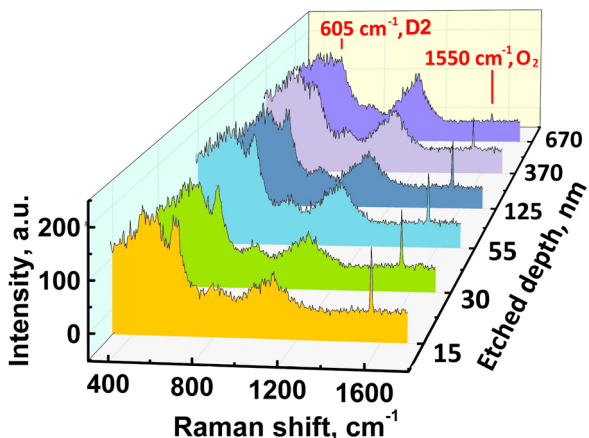


**Figure 5.** Raman spectra of sample no. 8 measured at different thicknesses of the removed layer that are etching depths.

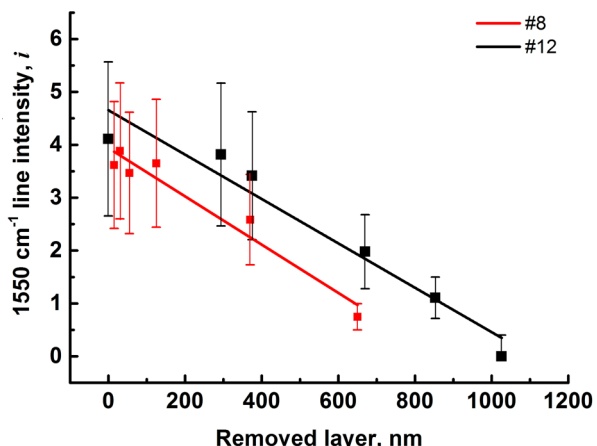


**Figure 6.** Intensity of the oxygen line in dependence on the thickness of the removed layer for samples nos. 8 and 12.

To evaluate  $O_2$  concentration, we use the proportion  $n = n_0 (i/i_{\text{suprasil}})(L/d)$ , where  $L \approx 1.5 \mu\text{m}$  is the length of Raman scattering, which is equal to the laser beam neck,  $d$  is the thickness of the oxygen-enriched layer, and  $n_0 \approx (8 \pm 3.5) \times 10^{17} \text{ cm}^{-3}$  (suprasil data<sup>30</sup>). Correction coefficient  $L/d$  accounts for the fact that the intensity of the glass matrix line is integrated over the length  $L$ , while the intensity of the  $O_2$  line over the thickness of  $O_2$ -enriched layer  $d$  is  $L > d$ . From Figure 6, it follows that the thickness of this layer,  $d$ , is  $d_8 \approx 900 \text{ nm}$  and  $d_{12} \approx 1050 \text{ nm}$  for the sample nos. 8 and 12, respectively. In Figure 4,  $i$  takes values  $i_8 \approx 3.3$  and  $i_{12} \approx 4.4$  for these samples that results in  $O_2$  concentrations  $n_8 \approx (2.3 \pm 1.9) \times 10^{20} \text{ cm}^{-3}$  and  $n_{12} \approx (2.5 \pm 1.8) \times 10^{20} \text{ cm}^{-3}$  for these samples. As the estimation on the order of magnitude, one can accept  $n \sim 3 \times 10^{20} \text{ cm}^{-3}$ . We emphasize that this estimate is of an order of magnitude only, and it is not intended to be more than that. In this evaluation, we do not consider the impact of changes in the symmetry because of the appearance of a polar axis in the poled glass, and the impact of the strong electric field frozen in the poled glass, as well as the effect of the molecular interaction on the probabilities of electron transitions in the poled layer. The influence of the glass matrix on the probability of electron transitions in the  $O_2$  molecule is assumed the same as in the selected for calibration Suprasil W1 silica glass. To reveal the influence of the frozen electric field on the spectra of poled glasses, the Raman spectra were recorded immediately after

poling of the samples and four months later. In soda-lime glasses, optical nonlinearity induced by the spatial charge normally decreases about twice<sup>31</sup> or even down to 10%<sup>32</sup> in three to four months. The comparison of the spectra has shown that there are no noticeable changes in the Raman spectra (i.e., built-in electric field in the subanodic glass region does not significantly affect the probability of the transitions).

For a comparison, we estimate the maximal concentration of  $O_2$ , which could be hypothetically generated in the studied glass if all mobile cations are removed from the poled volume, and the alkali silicate glass in this volume is converted to fused silica. In this hypothetical conversion, all NBO bonds transform to bridging ones and extra atoms of oxygen recombine and form oxygen molecules. For the formation of one  $O_2$  molecule, four alkali or two alkaline earth metal ions should be removed, resulting in two bridging oxygen bonds formation and no nonbridging bonds remaining. To keep electroneutrality, the second valent electron of each NBO atom should also be removed. In this case, the concentration of the interstitial  $O_2$  is determined by the sum of the concentrations of all removed ions, taking into account their valence:

$$\begin{aligned} n_{\max}(O_2) = & n(Na^+)/4 + n(K^+)/4 + n(Ca^{2+})/2 \\ & + n(Mg^{2+})/2 \end{aligned} \quad (1)$$

Using the data of Table 1, we get  $n_{\max}(O_2) \approx 3.5 \times 10^{21} \text{ cm}^{-3}$ , which is an order of magnitude higher than the value obtained in the experiment and 3 orders of magnitude higher than the concentration of  $O_2$  in the air under normal conditions,  $5.24 \times 10^{18} \text{ cm}^{-3}$ .

Thus, the study of the subsurface region of the poled glass showed that (1) molecular oxygen is formed in the cation-depleted subanodic layer, the thickness of which depends on the density of electric charge passed through the glass in poling and reaches about one micron; (2) the depth distribution of the interstitial molecular oxygen is nearly uniform, and its concentration is an order of magnitude less than the maximal one corresponding to hypothetical full relaxation of the glass structure to glassy silica; (3) under the craters formed in thermal poling on the glass surface, the concentration of the interstitial  $O_2$  exceeds one under the smooth surface of the poled region; (4) D2 band intensity in the subanodic layer of poled glass is abnormally high comparative to conventional silica glass; and (5) after annealing of the samples in the air at  $400^\circ\text{C}$  ( $673 \text{ K}$ ) for 1 h, the line of molecular oxygen disappears from Raman spectra.

#### 4. DISCUSSION

In 2010, Guimbretière and coauthors<sup>19</sup> promoted the idea that the mechanism of  $O_2$  formation in glass poling under blocking anode conditions includes a release of oxygen anions induced by structural rearrangements of the glass matrix. This release is followed by the formation of neutral  $O_2$  molecules and electron current toward the anode. Below, in the consideration of poling with blocking anode, we develop that idea, as well as propose and discuss in detail two versions of interstitial  $O_2$  generation, which differ in atomic oxygen diffusion mechanism through the glass matrix network. Contrary to ref 19, none of these versions supposes formation of the  $O_2$  molecule as a result of a direct interaction of two  $O^-$  ions with the emission of two electrons, since we consider this direct process to be low probable, and we propose a set of intermediate chemical reaction resulting in the interstitial molecular oxygen formation. Both versions are based

on the registered in our recent luminescence measurements<sup>33</sup> excess of oxygen in the form of nonbridging bonds in the poled layer consisting of nonstoichiometric silica glass. We, as well as noted in ref 19, suppose that the relaxation of mechanical stresses in this layer is crucial for molecular oxygen generation, but, contrary to the authors of refs 19 and 34, exclude anionic conductivity from the consideration. Here we assume that in the subanodic layer of a poled glass, where the formation of molecular oxygen occurs, there are no other defects, except NBO which are discharged. We do not consider the breaking of bridging oxygen bonds, diffusion of nonbridging bonds, or viscous flow of the glass that is the rejection of anionic species contribution and red/ox reactions at the electrode. These definitely should be considered for higher poling temperatures close to the glass transition. In that case, a viscous flow of the glass and, respectively, ionic conductivity, are activated. The latter could result in the formation of molecular oxygen through the reduction of oxygen ions on the anode.

It is worth noting that in the case of open anode poling, the registered injection of species originating from hydrogen<sup>7</sup> or nitrogen<sup>34</sup> and corresponding red/ox reactions<sup>34</sup> decrease the efficiency of the interstitial oxygen formation. Supposedly, this could be because of lower barriers of these reactions.

**4.1. Mechanism of Electron Transport in Subanodic Layer.** Starting from the pioneering study by Krieger<sup>21</sup> until recent research,<sup>19,34,35</sup> the possibility of electron transport in the course of glass poling has been under discussion. This electronic conductivity is supposed to be necessary for the formation of neutral oxygen.<sup>19</sup> Although the mechanism of electron transport is not a subject of this study, it needs to be considered here in the relation to the formation of molecular oxygen. One of the most probable mechanisms of this transport is hopping conductivity<sup>36</sup> with the hops from charged,  $\text{NBO}^-$ , to neutral NBO centers.

NBO center in silica glasses is a deep center which located  $\sim 2$  eV above the valence band edge.<sup>37,38</sup> In accordance with other studies,<sup>39,40</sup> the distance from the NBO level to the valence band edge equals  $\sim 0.3$  eV only. Currently, there are several models of this center and optical transitions in it (see ref 41 and references therein), but for the electron transport, the most important are the distance between the electronic levels of the neutral and charged centers, their position relative to the valence band edge, and the concentration of the centers. Common in all existing models of the center is that the highest energy nonbonding 2p orbital of NBO contains one unpaired electron. In this state, the NBO center is neutral and paramagnetic. If the second electron is added, the center becomes negatively charged and diamagnetic  $\text{NBO}^-$ , and the energy levels of the charged center shift up by  $\sim 2.5$  eV<sup>39</sup> or, according to another study, by  $\sim 1.5$  eV<sup>40</sup> relative to the neutral center. This is because of Coulomb repulsion of the electrons at the center (Hubbard shift in energy). If the concentration of the centers is high then their wave functions overlap and the impurity band is formed, which allows for the hopping mechanism of the charge transfer. Initially, after the removal of a cation, the center is charged; it is  $\text{NBO}^-$ .

During discharge of the closest to the anode  $\text{NBO}^-$  centers to the anodic electrode, neutral NBO centers (holes) appear in the ensemble of the charged centers  $\text{NBO}^-$ . These holes drift within the impurity band from the anode, thus providing conductivity of the poled subanodic layer.

Not all NBO can participate in the charge transfer, as a part of the adjacent bond pairs recombines after the discharge and

becomes excluded from the process. Even if all paired bonds recombine, that is  $\sim 50\%$  of nonbridging bonds are excluded, the average distance between the bonds in the remaining  $\sim 50\%$  of unpaired bonds is  $\langle R \rangle > 0.45\text{--}0.5$  nm. Since the localization radius,  $a_B$ , of the electron wave function is approximately equal to the half of Si–O bond length,  $l_{\text{Si}-\text{O}} \approx 0.16$  nm, we have  $a_B \approx 0.08$  nm. This localization provides the overlap of the wave functions of neighboring centers  $\sim \exp(2\langle R \rangle / a_B) \sim 10^{-5}$ , which is sufficient for electron hopping over the nearest neighbors.<sup>36</sup>

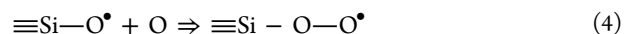
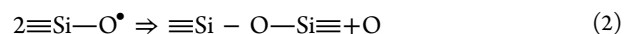
Another channel of decreasing the concentration of NBO capable of participation in the charge transfer is the capturing of atomic oxygen by NBO centers, which results in the formation of peroxide radicals. Note that low frequency absorption bands of NBO and peroxide radical centers substantially coincide and are located near 2 eV, both centers have the same oscillator strength<sup>42</sup> and similar energy levels structure in this energy region.<sup>38</sup> The similarity of NBO and peroxide radical centers is allowed, supposing that they can equally participate in the charge transfer.

Thus, on the basis of the available data on the energy levels of NBO and  $\text{NBO}^-$  centers,<sup>39,40</sup> one can suggest that high concentrations of these centers can result in the formation of two impurity bands in the range of energies  $\sim 0.3\text{--}2$  eV above the valence band edge with hole hopping conduction through the nearest neighbors within the empty Hubbard band. Note that the activation type of hole-hopping conductivity over neighboring sites has been observed at room temperature in the study of the hole mobility in thin layers of  $\alpha\text{-SiO}_2$  on silicon under a strong electric field.<sup>43</sup>

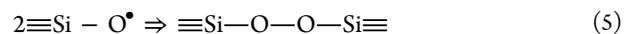
## 4.2. Atomic Oxygen Diffusion and $\text{O}_2$ Formation.

**4.2.1. Diffusion through Voids of the Network.** Poled glass can relax via increasing the glass matrix polymerization degree. This process is accompanied by  $\text{O}_2$  generation. Further we denote NBO in silica/silicate glasses as  $\equiv\text{Si}-\text{O}^\bullet$ . Here triple line corresponds to three bridging bonds in silicon–oxygen tetrahedra, and symbol “•” corresponds to an unpaired electron in the unfilled molecular orbital of the oxygen atom.

The behavior of oxygen during the polymerization of the matrix can be described with three main reactions:



Here reaction 2 is the recombination of two NBO resulting in the formation of free interstitial oxygen atom and a bridging bond, which increases the matrix polymerization; reaction 3 is the recombination of two oxygen atoms in the  $\text{O}_2$  molecule in the process of their diffusion within the glass matrix; reaction 4 is the capturing of an oxygen atom by NBO with the formation of a peroxide radical. We do not consider the peroxy-oxygen bonding



since the formation of the bridging bond reaction 2, which is shorter than the peroxide bond, corresponds to a more compact structure of glass network densified in poling. This densification is evidenced by the increase in the intensity of the Raman line corresponding to three-membered rings D2 in parallel with the increase in the density of electric charge passed in poling.

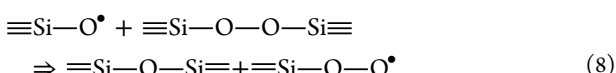
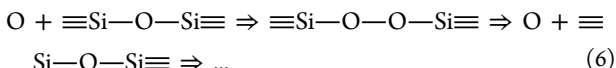
Modeling within the frames of cluster model shows<sup>44</sup> that reaction 2 is the exothermic one with the energy gain of 1.5 eV.

Supposedly, it is a stress-induced reaction. Reaction 3 is also exothermic with the energy gain of 5.1 eV, the gain being dependent on the size of cavity where the O<sub>2</sub> molecule forms.<sup>45</sup> This reaction is a diffusion-limited one. Experimental study<sup>46</sup> of atomic oxygen recombination in a silica glass has shown that in reaction 3, the molecular oxygen preferably forms at temperatures above 400 K, and the atomic oxygen diffusion coefficient satisfies the relation  $D = D_0 \exp(-E_a/kT)$ , where the activation energy  $E_a = 1.1$  eV and  $D_0 = 1 \times 10^{-3}$  cm<sup>2</sup>/s.<sup>46</sup> Reaction 4 is exothermic with an energy gain of 2.7 eV,<sup>47</sup> and supposedly, it is also diffusion-limited.

Peroxide radicals, the products of reaction 4, are thermally stable on the surface of a silica glass up to the temperature of 650 K.<sup>47</sup> Above 650 K, they decompose with the formation of oxygen atoms which, in their turn, react and form O<sub>2</sub> molecules. In the bulk of silica glasses, the peroxide radicals start to decompose at temperatures above 770 K.<sup>46</sup>

Since in our experiments, the poling was performed at 520 K, the accumulation of peroxide radicals according to the reaction 4 and the decrease in O<sub>2</sub> output were possible because of a competition of the reactions 4 and 3. The consideration above supposes the absence of other chemical interactions involved in the process that corresponds to the diffusion of atomic oxygen through voids of the glass network only.

**4.2.2. Diffusion through Sites of the Network.** Experimental data on the nature of atomic oxygen diffusion in glasses are contradictory (see ref 48 and references therein); however, it is established that the interstitial atomic oxygen can interact with network-bonded oxygen. Generally, this corresponds to the diffusion of atomic oxygen through sites of the network that is a kind of hopping mechanism. In theoretical studies,<sup>49,50</sup> a model of oxygen diffusion via the formation of peroxide bridges is proposed. Within the frames of that approach, the reactions 3 and 4 can be rewritten as



Here reaction 6 describes the diffusion of atomic oxygen through the matrix as subsequent actions of formation and decomposition of peroxide bridges, reaction 7 is the decomposition of a complex consisting of two peroxide bridges formed in their “collision” in the course of diffusion, which results in the formation of two bridging bonds and an interstitial (“free”) molecule of oxygen, and reaction 8 is a possible reaction of the peroxide radical formation as a result of a peroxide bridge and NBO “collision”. The sequence of the conversations, reaction 6, describes the diffusion of the peroxide bridge through the matrix and is a prerequisite for reaction 7 to occur. In accordance with existing estimates, the barrier of atomic oxygen (or peroxide bridge) diffusion in reaction 6 is equal to 1.3 eV (first-principles molecular dynamic calculation and  $\alpha$ -quartz supercell model<sup>49</sup>) or 1.9 eV (the density functional theory calculations<sup>51</sup>).

The authors of ref 51 relate this difference to the account of singlet–triplet character of the diffusion in their model: the fundamental state of the peroxide bridge is the singlet one, while the fundamental state of the oxygen atom is the triplet. It

was shown<sup>51</sup> that reaction 7 is exothermic with the barrier of ~1.6 eV. Reaction 8 was not discussed in literature. Since the highest barrier of 1.9 eV in the reactions 6 and 7 are related to the diffusion 6, formation of O<sub>2</sub> reaction 7 is a diffusion-limited reaction. The evaluation of O<sub>2</sub> formation rate in reaction 7 using the Arrhenius formula,  $v = v_0 \exp(-E/kT)$ , where  $v_0$  is characteristic phonon frequency,  $v_0 \sim 10^{13}$  s<sup>-1</sup>,  $\Delta E = 1.6$  eV is the barrier of the reaction, and  $T = 520$  K is poling temperature, gives  $v \approx 10^{-2}$  s<sup>-1</sup>. This rate is low but reasonable, as conventional poling duration is about tens of minutes. However, the activation energy, 1.9 eV, calculated in ref 51 is too high, while the barrier height of 1.3 eV calculated in ref 49 is in good agreement with the experimental data of 1–1.5 eV (see ref 46 and references therein).

Principally, both described above versions of O<sub>2</sub> formation, differing in atomic oxygen diffusion mechanism, do not contradict but rather complement each other.

**4.3. Structural Changes and Stress-Induced Bridging Oxygen Recombination.** The features of the structural changes of the glass matrix, which accompany O<sub>2</sub> formation, should be noted. As it is seen in Figure 2, under increasing the charge density passed in poling, the ratio of the D2 band intensity to the intensity of the matrix band at 400–550 cm<sup>-1</sup> increases in parallel with the intensity of the O<sub>2</sub> line. This indicates an increase in the quantity of three-membered rings in the poled glass. At the same time, the line D1 (495 cm<sup>-1</sup>), which is associated with four-membered rings, does not appear in the Raman spectra. Similar behavior of the D2 line was observed in SiO<sub>2</sub> films grown with the CVD technique<sup>52</sup> after their irradiation with neutrons<sup>22</sup> and also in thermally processed SiO<sub>2</sub> gels.<sup>53</sup> This means that in poling, the subanodic glass layer accumulates elastic energy sufficient for the formation of three-membered rings in the matrix, which is more energy-consuming than the formation of four-membered rings. Since this energy is stored after poling, nonrelaxed stresses exist in the poled glass. Another feature, the disappearance of the O<sub>2</sub> line after annealing the samples, is supposedly associated with the out-diffusion of the molecular oxygen from the glass. Indeed, the evaluation of characteristic diffusion length,  $L = (D_{\text{O}_2} t)^{1/2}$ , where  $D_{\text{O}_2} = 2.8 \times 10^{-4}$  exp( $-1.17/kT$ ) cm<sup>2</sup>/s, 1.17 eV is the activation energy of molecular oxygen diffusion in silica glass<sup>54</sup> for annealing duration  $t = 1$  h and temperature  $T = 400$  °C gives  $L = 300$  nm. This coincides with the thickness of containing O<sub>2</sub> subanodic layer,  $d \sim 600$ –1000 nm in order of magnitude. Supposedly, nonuniformities of the poled layer<sup>6</sup> could fasten this diffusion.

Presumably only NBO of neighboring tetrahedra are capable of the participation in reaction 2. This is because the diffusion of NBO can occur either via switching the bonds in viscous flow, which is possible either at temperatures close and above the glass transition temperature,<sup>55–58</sup> or under a high mechanical pressure, ~7 GPa.<sup>59</sup> Formation of a pair of neighboring nonbridging bonds occurs at sites which were left by divalent cations in poling. In accordance with the composition of our glass (see Table 1), divalent cations can be responsible for the formation of about 50% of all nonbridging bonds that is, in average, one pair of the neighboring bonds per six silicon tetrahedra.

As concerns the rest of ~50% of the nonbridging bonds which are left by alkali ions, they are randomly distributed within the poled volume of the glass. In accordance with Table

1, in the studied glass alkali ions form two nonbridging bonds per five tetrahedra in average. This allows supposing that one can neglect their participation in reaction 2. In glasses wherein the concentration of alkali ions is high, the probability of adjacent two locations of nonbridging bonds is higher, and they should also contribute to the reaction 2.

To initiate the reaction 2, two NBO should approach each other enough for bonding. Such approaching could be provided by the deformation of the angles of bridging Si—O—Si bonds because of mechanical stresses induced by cations drift (i.e., the reaction 2 can be induced by the stresses). It is worth noting that the rate of this reaction is also influenced by the glass temperature.

In poling, the source of the strongest stress is the frontier between the subanodic glass region depleted with cations and bulk glass, where the cations concentration is high. Measured thickness of this layer does not exceed 100–200 nm<sup>7</sup>, and the frontier moves toward the cathode with increasing the poling voltage and duration. The subanodic layer is also under an uniaxial compression caused by the electric field applied. Maximum pressure of this compression can be estimated from the magnitude of the electric field. In poling, it does not exceed 1 V/nm, see ref 60 and references therein. This allows evaluating maximally possible electrostatic pressure in the subanodic layer, which is equal to the volume density of electric field energy, as  $p = 0.5\epsilon_0\epsilon E^2 \approx 20$  MPa ( $\approx 200$  atm), where  $\epsilon_0$  is dielectric permittivity of vacuum,  $\epsilon \approx 5.5$  is relative dielectric permittivity of the glass, and  $E = 1$  V/nm is the maximal field.

Mechanical stresses at the poled–unpoled glass frontier can be estimated from the data on ion exchange in glasses. Assuming that the drift of cations induces stresses of the same order of magnitude as electrodiffusion or ion exchange we evaluate the stresses as  $\sim 1$  GPa.<sup>61,62</sup> It is common view that stress relaxation through a viscoelastic flow is possible only at temperatures close to the glass transition temperature,  $T_G$ . As the poling temperature in our experiment is substantially less than  $T_G$ , it can be assumed that the structural changes in the glass matrix are not associated with the viscoelastic flow, or at least this flow is not the main channel of the stress relaxation. Thus, in the absence of NBO diffusion, the pairs of adjacent nonbridging bonds are probably the main source of molecular oxygen. In the case of their complete recombination, without account for the formation of peroxide radicals, one can expect that about 50% of the maximally achievable concentration of O<sub>2</sub>,  $0.5n_{max} \approx 1.8 \times 10^{21}$  cm<sup>-3</sup> for the studied glass, is generated. The rest of the  $\sim 50\%$  of NBO formerly bonded to alkalis supposedly cannot take part in the recombination and stay in the matrix as defects. Thus, the glass matrix is not fully polymerized after the poling. It is worth noting that in the case of silica glass, the concentration of interstitial oxygen is determined by the concentration of defects and impurities as was considered by Skuja.<sup>30</sup>

## 5. CONCLUSION

The overall picture of interstitial molecular oxygen formation in poling of soda-lime silicate glasses in case of absence of nonbridging oxygen migration can be presented as follows. At the initial stage of the poling alkali ions displace from subanodic region of the glass and a layer of negative space charge containing charged nonbridging oxygen, NBO<sup>-</sup>, arises and grows in thickness. Under increasing voltage, less mobile divalent cations also leave the subanodic region. Once the voltage provides the electric field, which reaches the level

required for a significant activation of NBO<sup>-</sup> discharge through the electron transport to the anode, the field ceases to grow. This is followed by the formation of a frontier layer between the subanodic region of the glass depleted in cations and the bulk of the glass, where the cations concentration is high. Mechanical stresses generated at the frontier deform the angles of bridging Si—O—Si bonds of silicon tetrahedra without breaking the bonds. This deformation initiates the reaction of adjacent NBO recombination which increases the degree of the glass matrix polymerization. As the voltage applied to the glass increases, the frontier moves toward the cathode, leaving behind the polymerized matrix filled with O<sub>2</sub>, NBO, and, supposedly, peroxide radicals. The latter should be considered as a hypothesis, because, to our knowledge, no experimental studies aimed at the registration of the peroxide radical in poled glasses were reported. Since the poling frontier is the only source of molecular oxygen, the concentration of O<sub>2</sub> formed in the subanodic layer is about a constant. Evaluated in our experiments, O<sub>2</sub> concentration,  $\sim 3 \times 10^{20}$  cm<sup>-3</sup> less than in order of magnitude differs from the maximal one corresponding to the hypothetic recombination of all adjacent pairs of nonbridging bonds,  $1.8 \times 10^{21}$  cm<sup>-3</sup>. This indicates that both the reaction of the recombination of two NBO resulting in the formation of free interstitial oxygen atom and the reaction of the recombination of two oxygen atoms in O<sub>2</sub> molecule are sufficiently intensive. As follows from the measurements of the intensity of the oxygen line in the craters formed in poling, the output of O<sub>2</sub> in these reactions can be increased at a higher poling temperature. Thus, we treat the formation of interstitial molecular oxygen in the subanodic layer of alkali silicate glass subjected to thermal poling as a consequence of the modifications of the glass matrix. It results in a non-stoichiometry of the matrix composition due to an excess of nonbridging oxygen bonds in this layer, and the relaxation of the modified matrix causing an increase in its polymerization and densification through the formation of three-membered rings occurs. The concentration of molecular oxygen in the poled glass is mainly influenced by the initial concentration of adjacent pairs of nonbridging oxygen bonds formed by divalent cations in the glass. It is also significantly dependent on the rates of nonbridging oxygen recombination, atomic oxygen recombination, and, possibly, on atomic oxygen capturing by nonbridging oxygen with the formation of peroxide radicals.

## ■ ASSOCIATED CONTENT

### S Supporting Information

Complete author list of ref 22. The Supporting Information is available free of charge on the ACS Publications website at DOI: 10.1021/acs.jpcc.5b04513.

## ■ AUTHOR INFORMATION

### Corresponding Author

\*E-mail: lipovsky@spbau.ru. Tel: 8-812-4488591. Fax: 8-812-5435802.

### Notes

The authors declare no competing financial interest.

## ■ ACKNOWLEDGMENTS

The AFM studies were performed using the equipment of the Joint Research Centre: Material Science and Characterization in Advanced Technology (Ioffe Institute, St. Petersburg,

Russia). A.L. thanks the Russian Science Foundation for the support (Grant 14-22-00136).

## REFERENCES

- (1) Carlson, D. E.; Hang, K. W.; Stockdale, G. F. Electrode "Polarization" in Alkali-Containing Glasses. *J. Am. Ceram. Soc.* **1972**, *55*, 337–341.
- (2) Myers, R. A.; Mukherjee, N.; Brueck, S. R. Large Second-order Nonlinearity in Poled Fused Silica. *Opt. Lett.* **1991**, *16*, 1732–1734.
- (3) Qiu, M.; Pi, F.; Orriols, G.; Bibiche, M. Signal Damping of Second-Harmonic Generation in Poled Soda-Lime Silicate Glass. *J. Opt. Soc. Am. B* **1998**, *15*, 1362–1365.
- (4) Garcia, F. C.; Carvalho, I. C. S.; Hering, E.; Margulis, W.; Lesche, B. Inducing a Large Second-Order Optical Nonlinearity in Soft Glasses by Poling. *Appl. Phys. Lett.* **1998**, *72*, 3252–3254.
- (5) de Vekey, R. C.; Majumdar, A. J. Effect of Electric Field on Phase Separation of Glass. *Nature* **1970**, *225*, 172–173.
- (6) An, H.; Fleming, S. Second-Order Optical Nonlinearity and Accompanying Near-Surface Structural Modifications in Thermally Poled Soda-Lime Silicate Glasses. *J. Opt. Soc. Am. B* **2006**, *23*, 2303–2309.
- (7) Lepienski, C. M.; Giacometti, J. A.; Leal Ferreira, G. F.; Freire, F. L., Jr.; Achete, C. A. Electric Field Distribution and Near-Surface Modifications in Soda-Lime Glass Submitted to a DC Potential. *J. Non-Cryst. Solids* **1993**, *159*, 204–212.
- (8) Margulis, W.; Laurell, F. Fabrication of Waveguides in Glasses by a Poling Procedure. *Appl. Phys. Lett.* **1997**, *71*, 2418–2420.
- (9) Dussauze, M.; Kamitsos, E. I.; Fargin, E.; Rodriguez, V. Refractive Index Distribution in the Non-Linear Optical Layer of Thermally Poled Oxide Glasses. *Chem. Phys. Lett.* **2009**, *470*, 63–66.
- (10) Takagi, H.; Miyazawa, S.-i.; Takahashi, M.; Maeda, R. Electrostatic Imprint Process for Glass. *Appl. Phys. Express* **2008**, *1*, 024003.
- (11) Brunkov, P. N.; Melekhin, V. G.; Goncharov, V. V.; Lipovskii, A. A.; Petrov, M. I. Submicron-Resolved Relief Formation in Poled Glasses and Glass–Metal Nanocomposites. *Tech. Phys. Lett.* **2008**, *34*, 1030–1033.
- (12) Redkov, A. V.; Melehin, V. G.; Statcenko, V. V.; Lipovskii, A. A. Nanoprofiling of Alkali-Silicate Glasses by Thermal Poling. *J. Non-Cryst. Solids* **2015**, *409*, 166–169.
- (13) Margulis, W.; Laurell, F. Interferometric Study of Poled Glass under Etching. *Opt. Lett.* **1996**, *21*, 1786–178.
- (14) Canagasabey, A.; Corbari, C.; Zhang, Z.; Kazansky, P. G.; Ibsen, M. Broadly Tunable Second-Harmonic Generation in Periodically Poled Silica Fibers. *Opt. Lett.* **2007**, *32*, 1863–1865.
- (15) Kazansky, P. G.; Russell, P. S. J.; Dong, L.; Pannell, C. N. Pockels effect in thermally poled silica optical fibres. *Electron. Lett.* **1995**, *31*, 62–63.
- (16) Brennand, A. L. R.; Wilkinson, J. S. Planar Waveguides in Multicomponent Glasses Fabricated by Field-Driven Differential Drift of Cations. *Opt. Lett.* **2002**, *27*, 906–908.
- (17) Ikutame, N.; Kawaguchi, K.; Ikeda, H.; Sakai, D.; Harada, K.; Funatsu, S.; Nishii, J. Low-Temperature Fabrication of Fine Structures on Glass Using Electrical Nanoimprint and Chemical Etching. *J. Appl. Phys.* **2013**, *114*, 083514.
- (18) Dussauze, M.; Rodriguez, V.; Lipovskii, A.; Petrov, M.; Smith, C.; Richardson, K.; Cardinal, T.; Fargin, E.; Kamitsos, E. I. How Does Thermal Poling Affect the Structure of Soda-Lime Glass? *J. Phys. Chem. C* **2010**, *114*, 12754–12759.
- (19) Guimbretière, G.; Dussauze, M.; Rodriguez, V.; Kamitsos, E. I. Correlation Between Second-Order Optical Response and Structure in thermally Poled Sodium Niobium-Germanate Glass. *Appl. Phys. Lett.* **2010**, *97*, 171103.
- (20) Carlson, D. E.; Hang, K. W.; Stockdale, G. F. Electrode "Polarization" in Alkali-Containing Glasses. *J. Am. Ceram. Soc.* **1972**, *55*, 337–341.
- (21) Krieger, U. K.; Lanford, W. A. Field Assisted Transport of Na<sup>+</sup>, Ca<sup>2+</sup> Ions and Electrons in Commercial Soda-Lime Glass: I. Experimental. *J. Non-Cryst. Solids* **1988**, *102*, 50–61.
- (22) Weber, W. J.; Ewing, R. C.; Angell, C. A.; Arnold, G. W.; Cormack, A. N.; Delaye, J. M.; Griscom, D. L.; Hobbs, L. W.; Navrotsky, A.; Price, D. L.; et al. Radiation Effects in Glasses Used Immobilization of High-Level Waste and Plutonium Disposition. *J. Mater. Res.* **1997**, *12*, 1948–1978.
- (23) Bressel, L.; de Ligny, D.; Gamaly, E.; Rode, A.; Juodkazis, S. Observation of O<sub>2</sub> Inside Voids Formed in GeO<sub>2</sub> Glass by Tightly-Focused fs-Laser Pulses. *Opt. Mater. Express* **2011**, *1*, 1150–1157.
- (24) Menzel-Gläser. <http://www.menzel.de/> (accessed May 7, 2015).
- (25) Kaneko, T. Dilatation of Glass by Field-Assisted Ion Exchange. *J. Mater. Sci. Lett.* **1986**, *5*, 1011–1012.
- (26) Galeener, F. L. Planar Rings in Vitreous Silica. *J. Non-Cryst. Solids* **1982**, *49*, 53–62.
- (27) Krupenie, H. The Spectrum of Molecular Oxygen. *J. Phys. Chem. Ref. Data* **1972**, *1*, 423–534.
- (28) Skuja, L.; Guttler, B. Detection of Interstitial Oxygen Molecules in SiO<sub>2</sub> Glass by Direct Photoexcitation of the Infrared Luminescence of Singlet O<sub>2</sub>. *Phys. Rev. Lett.* **1996**, *77*, 2093–2096.
- (29) Boizot, D.; Petite, G.; Ghaleb, D.; Reynard, B.; Calas, G. Raman Study of β-irradiated Glasses. *J. Non-Cryst. Solids* **1999**, *268*, 269–272.
- (30) Skuja, L.; Guttler, B.; Schiel, D.; Silin, A. R. Quantitative Analysis of the Concentration of Interstitial O<sub>2</sub>Molecules in SiO<sub>2</sub> Glass Using Luminescence and Raman Spectrometry. *J. Appl. Phys.* **1998**, *83*, 6106–6110.
- (31) Moura, A. L.; de Araujo, M. T.; Vermelho, M. V. D.; Aitchison, J. S. Improved Stability of the Induced Second-Order Nonlinearity in Soft Glass by Thermal Poling. *J. Appl. Phys.* **2006**, *100*, 033509.
- (32) Garcia, I. F. C.; Carvalho, C. S.; Hering, E.; Margulis, W.; Lesche, B. Inducing a Large Second-Order Optical Nonlinearity in Soft Glasses by Poling. *Appl. Phys. Lett.* **1998**, *72*, 3252–3254.
- (33) Afrosimov, V. V.; Ber, B.; Ya; Zhurikhina, V. V.; Zamoryanskaya, M. V.; Kazantsev, D. Yu.; Kolesnikova, E. V.; Lipovskii, A. A.; Petrov, M. I.; Melekhin, V. G. Mass Transfer in Thermo Electric Field Modification of Glass–Metal Nanocomposites. *Tech. Phys.* **2010**, *55*, 1600–1609.
- (34) Cremoux, T.; Dussauze, M.; Fargin, E.; Cardinal, T.; Talaga, D.; Adamietz, F.; Rodriguez, V. Trapped Molecular and Ionic Species in Poled Borosilicate Glasses: Toward a Rationalized Description of Thermal Poling in Glasses. *J. Phys. Chem. C* **2014**, *118*, 3716–3723.
- (35) Corbari, C.; Ajitdoss, L.; Carvalho, I.; Deparis, O.; Mezzapesa, F.; Kazansky, P.; Sakaguchi, K. The Problem of Achieving High Second-Order Nonlinearities in Glasses: The Role of Electronic Conductivity in Poling of High Index Glasses. *J. Non-Cryst. Solids* **2010**, *356*, 2742–2749.
- (36) Mott, N. F.; Devis, E. A. *Electronic Processes in Non-Crystalline Materials*; Oxford Classic Texts in the Physical Sciences; Oxford University Press: Oxford, U.K., 1979.
- (37) Pacchioni, G.; Ierano, G. Ab Initio Theory of Optical Transitions of Point Defects in SiO<sub>2</sub>. *Phys. Rev. B: Condens. Matter Mater. Phys.* **1998**, *57*, 818–832.
- (38) O'Reilly, E. P.; Robertson, J. Theory of Defects in Vitreous Silicon Dioxide. *Phys. Rev. B: Condens. Matter Mater. Phys.* **1983**, *27*, 3780–3795.
- (39) Martinez, U.; Giordano, L.; Pacchioni, G. Nature of Point Defects on SiO<sub>2</sub>/Mo(112) thin Films and Their Interaction with Au Atom. *J. Phys. Chem. B* **2006**, *110*, 17015–17023.
- (40) Bakos, T.; Rashkeev, S. N.; Pantelides, S. T. Optically Active Defects in SiO<sub>2</sub>: The Nonbridging Oxygen Center and the Interstitial OH Molecules. *Phys. Rev. B: Condens. Matter Mater. Phys.* **2004**, *70*, 075203.
- (41) Suzuki, T.; Skuja, L.; Kajihara, K.; Hirano, M.; Kamiya, T.; Hosono, H. Electronic Structure of Oxygen Dangling Bond in Glassy SiO<sub>2</sub>: The Role of Hyperconjugation. *Phys. Rev. Lett.* **2003**, *90*, 186404.
- (42) Skuja, L. Optically Active Oxygen-Deficiency-Related Centers in Amorphous Silicon Dioxide. *J. Non-Cryst. Solids* **1998**, *239*, 16–48.
- (43) Hughes, R. C. Time-Resolved Hole Transport in α-SiO<sub>2</sub>. *Phys. Rev.* **1977**, *15*, 2012–2020.

- (44) Pacchioni, G.; Ierano, G. Ab Initio Formation Energies of Point Defects in Pure and Ge-doped SiO<sub>2</sub>. *Phys. Rev. B: Condens. Matter Mater. Phys.* **1997**, *56*, 7304–7312.
- (45) Bakos, T.; Rashkeev, S. N.; Pantelides, S. T. H<sub>2</sub>O and O<sub>2</sub> Molecules in Amorphous SiO<sub>2</sub>: Defect Formation and Annihilation Mechanisms. *Phys. Rev. B: Condens. Matter Mater. Phys.* **2004**, *69*, 195206.
- (46) Kajihara, K.; Miura, T.; Kamioka, H.; Aiba, A.; Uramoto, M.; Morimoto, Y.; Hirano, M.; Skuja, L.; Hosono, H. Diffusion and Reactions of Interstitial Oxygen Species in Amorphous SiO<sub>2</sub>: a Review. *J. Non-Cryst. Solids* **2008**, *354*, 224–232.
- (47) Radzig, V. A. Defects on the Silica Surface: Structure and Reactivity. In *Chemical Phenomena in Thin Films and at Solid Surfaces*; Elsevier: Amsterdam, 2007; 34, Chapter 7, pp 231–345.
- (48) Doremus, R. H. Transport of Oxygen in Silicate Glasses. *J. Non-Cryst. Solids* **2004**, *349*, 242–247.
- (49) Hamann, D. R. Diffusion of Atomic Oxygen in SiO<sub>2</sub>. *Phys. Rev. Lett.* **1998**, *81*, 3447–3450.
- (50) Szymanski, M. A.; Shluger, A. L.; Stoneham, A. M. Role of Disorder in Incorporation Energies of Oxygen Atoms in Amorphous Silica. *Phys. Rev. B: Condens. Matter Mater. Phys.* **2001**, *63*, 224207.
- (51) Orellana, W.; da Silva, A. J. R.; Fazzio, A. Oxygen-Induced Atomic Desorption in Oxynitrides: Density Functional Calculations. *Phys. Rev. B: Condens. Matter Mater. Phys.* **2005**, *72*, 205316.
- (52) Devine, R. A. B.; Marchand, M. Evidence for Structural Similarities between Chemical Vapor Deposited and Neutron Irradiated SiO<sub>2</sub>. *Appl. Phys. Lett.* **1993**, *63*, 619–621.
- (53) Brinker, C. J.; Brow, R. K.; Tallant, D. R.; Kirkpatrick, R. J. Surface Structure and Chemistry of High Surface Area Silica Gels. *J. Non-Cryst. Solids* **1990**, *120*, 26–33.
- (54) Revesz, A. G.; Scheffer, H. A. The Mechanism of Oxygen Diffusion in Vitreous SiO<sub>2</sub>. *J. Electrochem. Soc.* **1982**, *129*, 357–361.
- (55) Filipovich, V. N. Theory of Oxygen Self-Diffusion in Glassy SiO<sub>2</sub>, GeO<sub>2</sub>. *Fiz. i Khim. Stekla* **1978**, *4*, 22–30 (in Russian).
- (56) Myuller, R. L. The Valence Theory of Viscosity and Fluidity in the Critical Temperature Range for Refractory Glass-Forming Materials. *Zh. Prikl. Khim.* **1955**, *28*, 1077–1087 (in Russian).
- (57) Nemilov, S. V. *Thermodynamic and Kinetic Aspects of Vitreous State*; CRC Press: Boca Raton, 1995.
- (58) Mott, N. F. The Viscosity of Vitreous Silicon Dioxide. *Philos. Mag. B* **1987**, *56*, 257–262.
- (59) Nomura, K.; Chen, Y. Ch.; Kalia, R. K.; Nakano, A.; Vashishta, P. Defect Migration and Recombination in Nanoindentation of Silica Glass. *Appl. Phys. Lett.* **2011**, *99*, 111906.
- (60) Lipovskii, A. A.; Melehin, V. G.; Petrov, M. I.; Svirko, Yu. P.; Zhurikhina, V. V. Bleaching vs Poling: Comparison of Electric Field Induced Phenomena in Glasses and Glass-Metal Nanocomposites. *J. Appl. Phys.* **2011**, *109*, 011101.
- (61) Mazzoldi, P.; Carturan, S.; Quaranta, A.; Sada, C.; Sglavo, V. M. Ion Exchange Process: History, Evolution and Applications. *Revista Del Nuovo Cimento* **2013**, *36*, 397–460.
- (62) Karlsson, S.; Jonson, B.; Stalhandske, C. The Technology of Chemical Glass Strengthening. A Review. *Glass Technol.: Eur. J. Glass Sci. Technol. A* **2010**, *51*, 41–54.